



High-pressure phase transition in Mn_2O_3 : Application for the crystal structure and preferred orientation of the CaIrO_3 type

Javier Santillán,^{1,2} Sang-Heon Shim,¹ Guoyin Shen,^{3,4} and Vitali B. Prakapenka³

Received 27 March 2006; revised 25 May 2006; accepted 22 June 2006; published 4 August 2006.

[1] Our X-ray diffraction measurements reveal that Mn_2O_3 undergoes a phase transition to the CaIrO_3 type, which is proposed for the post-perovskite in MgSiO_3 , at 27–38 GPa and 300 K, bypassing the other phase transitions observed in sesquioxides. Small distortions in the polyhedra after the transition indicate that the Jahn-Teller effect, which is strong at ambient conditions, is suppressed during the transition. The CaIrO_3 -type phase exhibits strong preferred orientation of the (010) plane perpendicular to the loading axis before annealing whereas preferred orientation of the (100) and (110) planes was observed after annealing. The pre-annealing texture may result from either the deformation under strong differential stresses or the phase transition. The post-annealing texture may be related to either lower differential stresses or thermal annealing. Our result shows that the texture of the CaIrO_3 type can be sensitive to phase transition and annealing as well as differential stresses.
Citation: Santillán, J., S.-H. Shim, G. Shen, and V. B. Prakapenka (2006), High-pressure phase transition in Mn_2O_3 : Application for the crystal structure and preferred orientation of the CaIrO_3 type, *Geophys. Res. Lett.*, 33, L15307, doi:10.1029/2006GL026423.

1. Introduction

[2] Phase transitions in sesquioxide minerals (e.g., corundum, hematite, and eschelite) have long been the subject of interest due to the relevance of their high-pressure (P) structures to mantle minerals [e.g., Reid and Ringwood, 1969]. From experiments [e.g., Funamori and Jeanloz, 1997; Shim *et al.*, 2004b; Ono *et al.*, 2004; Lin *et al.*, 2004] and first-principles calculations [e.g., Thomson *et al.*, 1996], a general sequence of phase transitions has been established for sesquioxides at high P : corundum-type \rightarrow Rh_2O_3 -II or perovskite-type. A sequence of phase transition for MgSiO_3 with pressure is: pyroxene \rightarrow ilmenite or garnet (depending on temperature) \rightarrow perovskite. It is notable that the ilmenite type has essentially a cation-ordered corundum structure. More recent works have shown that hematite and corundum further transform to the CaIrO_3 -type ($Cmcm$) phases at 60 and 160 GPa at high temperatures, respectively [Ono and Ohishi, 2005; Oganov and Ono, 2005]. This is geophys-

ically important because MgSiO_3 perovskite, the dominant lower-mantle mineral, also transforms to a CaIrO_3 -type phase at 120 GPa [Murakami *et al.*, 2004].

[3] Bixbyite, $(\text{Mn}_{1-x}\text{Fe}_x)_2\text{O}_3$, is unique among sesquioxide minerals in that it has the C-type rare earth structure instead of the corundum-type structure at ambient conditions [Geller, 1971]. In Mn endmember (α - Mn_2O_3), Mn^{3+} exists in five different crystallographic sites, each surrounded by a highly distorted octahedron of O atoms. This distortion, known as the Jahn-Teller (JT) distortion, is due to the loss of degeneracy in the $3d$ -orbitals when Mn^{3+} is coordinated by six O atoms. It has been predicted that suppression of the JT effect with compression would make bixbyite transform to a corundum-type phase [Prewitt *et al.*, 1969] and then follow the sequence of high- P transitions observed in other sesquioxide minerals. Prewitt *et al.* [1969] found that Mn_2O_3 transitions to a distorted C-type structure at 1573 K and 6.5 GPa. Syono *et al.* [1985] reported a phase transition at 29 GPa. Yamanaka *et al.* [2005] confirmed the transition and tentatively assigned a monoclinic unit cell to the high- P phase. However, the crystal structure of the high- P phase is not known.

[4] Here we report that Mn_2O_3 transforms directly to the CaIrO_3 type. We focus on distortions in the crystal structure, phase transition, and lattice preferred orientation of the CaIrO_3 -type phase, which provides insights on properties of the post-perovskite phase in MgSiO_3 .

2. Experimental Techniques

[5] Pure synthetic Mn_2O_3 powder was placed in a hole of a pre-indented Re gasket with ruby grains near the edge of the hole to serve as a pressure calibrant [Mao *et al.*, 1986]. Diamond-anvil cells (DACs) were prepared with 500- μm culet anvils. The piston diamond was epoxied onto a cubic BN seat to allow for diffraction measurement up to 23° 2θ . Argon was loaded as a pressure medium.

[6] X-ray diffraction patterns were collected up to 40.4 GPa at the GSECARS sector of the Advanced Photon Source. At 40.4 GPa, in order to anneal differential stresses, the edge of the sample was laser heated to less than 1000 K. We did not scan laser beams at the center of the sample where post-annealing diffraction patterns were obtained. Thus, the temperature of the X-rayed area should not exceed a few hundred kelvins during annealing. Diffraction images were collected using an imaging plate. Images were processed using the FIT2D application [Hammersley, 1997]. The sample-to-detector distance and tilt of the imaging plate were corrected by measuring the diffraction patterns of CeO_2 . We corrected for the attenuation of diffracted X-ray beams through a cBN seat. Cell parameters were refined using the UNITCELL program [Holland and

¹Department of Earth, Atmospheric, and Planetary Sciences, Massachusetts Institute of Technology, Cambridge, Massachusetts, USA.

²Now at Ahura Corporation, Wilmington, Massachusetts, USA.

³GSECARS, University of Chicago, Chicago, Illinois, USA.

⁴Now at HPCAT, Argonne National Laboratory, Argonne, Illinois, USA.

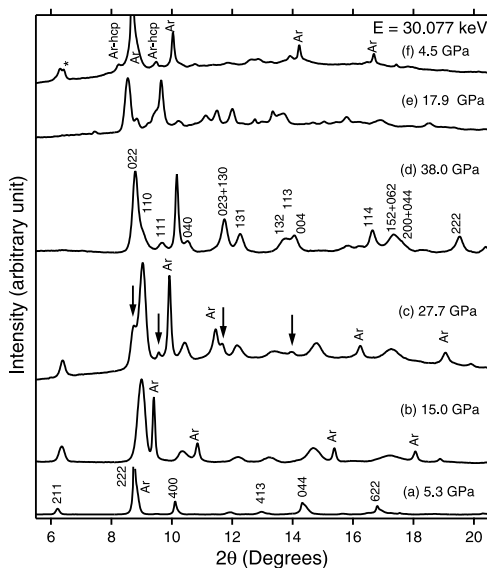


Figure 1. X-ray diffraction patterns of Mn_2O_3 at high P . The indexed lines in (a) and (d) are for the major diffraction lines of $\alpha\text{-Mn}_2\text{O}_3$ and CaIrO_3 -type phases, respectively. The arrows in (c) indicate new diffraction lines observed during the phase transition. The asterisk in (f) indicates a spotty ring from a heating product.

Redfern, 1997]. Rietveld refinements of diffraction patterns were carried out using the GSAS package [Larson and Von Dreele, 1988]. A spherical harmonics function [Bunge, 1983] for the cylindrical sample symmetry was used for fitting the preferred orientation effect.

3. Results

[7] Mn_2O_3 diffraction lines broaden with an increase of pressure even with the soft Ar pressure medium, while the

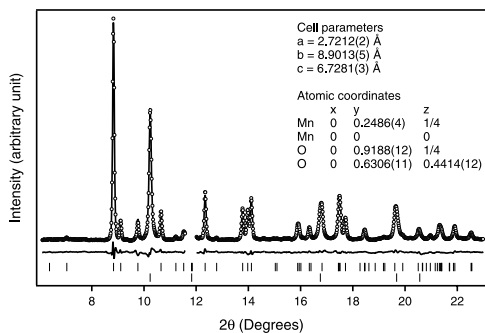


Figure 2. Rietveld refinement result of the diffraction pattern measured after annealing at 40.4 GPa ($R_{wp} = 0.085$). The circles are the observed intensities and the line behind the circles is the calculated diffraction pattern. Differences between observed and calculated intensities are shown below the pattern. The bars represent peak positions for the CaIrO_3 -type phase (top) and argon (bottom). Due to severe overlap of diffraction lines between Ar and Mn_2O_3 , we do not include the data points at $11.6\text{--}12.0^\circ 2\theta$ in the refinement.

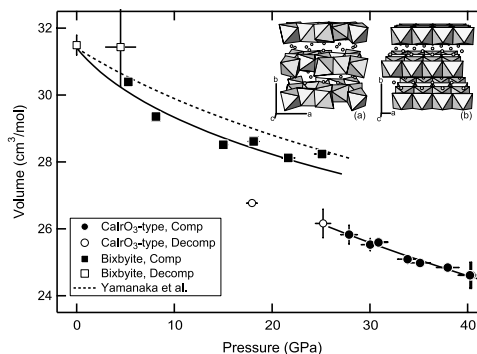


Figure 3. Volume of Mn_2O_3 at high P . The circle and square symbols represent low- P and CaIrO_3 -type phases, respectively. Solid and open symbols represent data points from compression and decompression, respectively. The error bars are 1σ estimated uncertainties. The compressional curve reported by *Yamanaka et al.* [2005] is shown in a dashed line. The solid lines to guide the eye. The insets show the crystal structures of $\alpha\text{-Mn}_2\text{O}_3$ (a) and the CaIrO_3 type (b).

Ar peaks remain sharp (Figures 1a and 1b). At 27.7 GPa, several new peaks appear (Figure 1c). However, the 211 peak, diagnostic of the low- P phase, remains to 38.0 GPa, at which the phase transition completes (Figure 1d). This is consistent with *Yamanaka et al.* [2005].

[8] At 40.4 GPa, we laser annealed the sample resulting in a pronounced sharpening of all the peaks, but not in the appearance of additional new peaks (Figure 2). This suggests that no phase separation or temperature-induced phase transition occurs during annealing. In addition, the diffraction rings in the 2D image remain continuous and do not become spotty, indicating little or no crystal growth is induced during the annealing. The pressure slightly drops after annealing (0.2 GPa). At least 25 peaks are clearly resolved after annealing (Figure 2) and they are indexed well with an orthorhombic unit cell. *Yamanaka et al.* [2005] tentatively assigned a monoclinic unit cell for the high- P phase. No angles deviate significantly from 90° in our monoclinic unit-cell fitting. In *Yamanaka et al.* [2005]'s study, diffraction lines are significantly broader and only 11 diffraction lines were used for unit-cell determination. The observed diffraction pattern of the high- P phase agrees well with that of the CaIrO_3 type (Figure 2), which has been proposed for the crystal structure of the post-perovskite phase in MgSiO_3 [Murakami et al., 2004]. We perform Rietveld refinements on diffraction patterns by taking the CaIrO_3 type as a starting model (Figure 2). We observe a pronounced preferred orientation effect in the pre-annealing patterns that becomes smaller in the post-annealing patterns. The background-subtracted residual value ranges from 0.055 to 0.085. Upon decompression, the diffraction patterns indicate that a mixed phase region exists between 30 and 4.5 GPa. All the diffraction lines observed for the recovered sample can be explained by $\alpha\text{-Mn}_2\text{O}_3$, indicating that the high- P phase is not quenchable.

[9] The volume of the low- P phase in our measurements is lower by 2% than *Yamanaka et al.* [2005] at high P (Figure 3). We note that we used Ar as a pressure medium

Table 1. Quadratic Elongation of Polyhedra in α - Mn_2O_3 at 1 bar [Geller, 1971] and $CaIrO_3$ -Type Phases in Mn_2O_3 at 40.2 GPa [From This Work], Fe_2O_3 at 68 GPa [Ono and Ohishi, 2005], and $MgSiO_3$ at 121 GPa [Murakami et al., 2004]

Coordination	α - Mn_2O_3	$CaIrO_3$ -Type		
		Mn_2O_3	Fe_2O_3	$MgSiO_3$
OCT1 ^a	1.0094(71)	1.0055(71)	1.0219(72)	1.0026(70)
OCT2	1.0094(71)			
OCT3	1.0780(76)			
OCT4	1.0774(76)			
OCT5	1.0765(76)			
BTP ^b		0.9273(52)	0.9291(52)	0.9258(52)

^aOctahedra.

^bBicapped trigonal prisms.

whereas Yamanaka et al. [2005] used a methanol-ethanol mixture which becomes non-hydrostatic above 10–15 GPa. The volume decreases by 8% across the phase transition between 25.1 GPa and 27.9 GPa.

4. Discussion

[10] The stability of the C-type structure in bixbyite at ambient conditions has been attributed to strong distortions in the MnO_6 octahedra resulting from the Jahn-Teller (JT) effect [Geller, 1971]. Therefore, if the JT effect is suppressed by compression, bixbyite would follow a sequence of the phase transitions found in other sesquioxide minerals without the JT distortion. Escolite [Shim et al., 2004b], hematite [Ono et al., 2004], and corundum [Lin et al., 2004] undergo a phase transition from the corundum-type to an orthorhombic (either Rh_2O_3 -II or perovskite-type) phase at 30, 35, and 90 GPa, respectively. It has recently been reported that hematite and corundum further transform to the $CaIrO_3$ type at 60 GPa and 160 GPa, respectively [Ono and Ohishi, 2005; Oganov and Ono, 2005], which is proposed for the crystal structure of the post-perovskite phase in $MgSiO_3$.

[11] However, we find that Mn_2O_3 bypasses the phase transitions to the corundum- and perovskite- or Rh_2O_3 -II-type phases. Instead, it directly transforms to the $CaIrO_3$ type, which appears after the perovskite type in $MgSiO_3$ [Murakami et al., 2004; Shim et al., 2004a; Oganov and Ono, 2004] and after an orthorhombic phase in Fe_2O_3 [Ono and Ohishi, 2005]. Another interesting observation is that the transition occurs without heating. So far, the phase transitions to the $CaIrO_3$ type have been observed after heating to at least 2000 K, such as $MgSiO_3$ [Murakami et al., 2004; Oganov and Ono, 2004; Shim et al., 2004b], Al_2O_3 [Oganov and Ono, 2005], and Fe_2O_3 [Ono and Ohishi, 2005]. This indicates a large kinetic energy barrier for the phase transition to the $CaIrO_3$ type except for Mn_2O_3 .

[12] The crystal structure data for $CaIrO_3$ -type Mn_2O_3 obtained from Rietveld refinements allow us to infer the existence of the JT effect through the distortions of the polyhedra. We calculate the quadratic elongation [Robinson et al., 1971] as shown in Table 1: the more the deviation of the quadratic elongation from 1, the larger the distortion. Compared to the octahedra in α - Mn_2O_3 , the distortion of the octahedron in the $CaIrO_3$ -type phase is negligible. Although the quadratic elongation of the MnO_8 bicapped

trigonal prism deviates significantly from 1, this is mainly because of the difference in shape between a bicapped trigonal prism and an ideal 8-fold geometry, i.e., cubic. The degree of distortion in the bicapped trigonal prism in Mn_2O_3 is similar to those in other $CaIrO_3$ -type materials without the JT distortion (Table 1).

[13] It is possible that the JT effect may be suppressed gradually with compression. However, a single crystal X-ray diffraction study for bixbyite with 40% Fe up to 9 GPa has shown no clear change in the quadratic elongation with P within the uncertainty [Yamanaka et al., 2005]. An alternative possibility is suppression of the JT distortion during the phase transition to the $CaIrO_3$ type. Although the JT effect is strong for octahedrally coordinated Mn^{3+} in the high-spin configuration, it should not exist in the low-spin configuration [Burns, 1993]. Thus, the observed absence of the JT distortion in the octahedra after the phase transition may result from a change in the spin configuration. Indeed, Fe^{3+} in hematite undergoes a change to a low-spin state at 60 GPa [Badro et al., 2002]. Furthermore, the bicapped trigonal prism configuration is not an efficient way to accommodate the JT effect compared with the octahedral coordination [Burns, 1993]. The charge disproportionation of $2Mn^{3+}$ to Mn^{2+} and Mn^{4+} can also result in the suppression of the JT effect. Because Mn^{4+} is smaller and Mn^{2+} receives zero crystal field splitting energy in octahedral coordination, Mn^{4+} would enter into the octahedral site. However, Mn^{4+} ($3d^3$) in the octahedral site would not show any JT distortion, because no electrons enter in e_g orbitals [Burns, 1993]. However, the possible association of the phase transition to the $CaIrO_3$ type in Mn_2O_3 with either change in the spin configuration or the charge disproportionation remains to be examined using a more direct probe.

[14] Although the JT distortion is apparently suppressed, Mn_2O_3 does not follow the sequence of the phase transitions found in other sesquioxide minerals without the JT distortions. We recognize some similarities between the C-type and $CaIrO_3$ -type structures (insets in Figure 3). Bixbyite is made up of alternating layers of the less distorted (Mn1, Mn2, and Mn5) and the more distorted (Mn3 and Mn4) octahedra (Table 1). Although Mn5 has lower site symmetry, it shows slightly lower distortion than the other two lower symmetry octahedra (Mn3 and Mn4). On the other hand, the crystal structure of the $CaIrO_3$ type consists of alternating layers of the octahedra and the bicapped trigonal prisms. Thus, perhaps the most energetically favorable way is to re-organize the intra-layer structure while largely maintaining the 2D nature of the crystal structure during the phase transition. This may explain such a low kinetic barrier for the transition to the $CaIrO_3$ type in Mn_2O_3 .

[15] Before annealing, the intensities of the 110 and 131 peaks for the $CaIrO_3$ type are larger and smaller than those expected for randomly oriented crystals, respectively. However, after annealing, the 110 peak intensity becomes smaller than expected, while the 131 peak intensity becomes comparable to an expected value. In Rietveld analysis, we refine the preferred orientation (Figure 4). The $CaIrO_3$ type shows strong preferred orientation of the (010) plane perpendicular to the loading axis of the DAC (or the plane normal aligning along the loading axis). However, after annealing, we found that 010 becomes

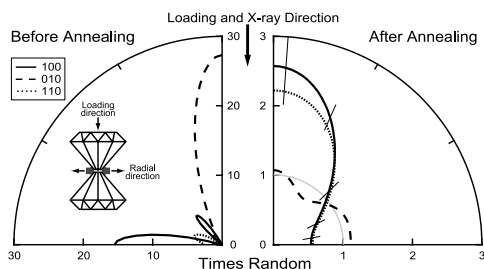


Figure 4. Distribution of the poles of the planes in the $CaIrO_3$ -type phase before and after annealing. The radial axis represents multiples of a random distribution. The vertical direction is the loading direction and the horizontal direction is the radial direction of DAC (as shown in the inset). The error bars are 2σ estimated uncertainties. Random distribution is shown by a gray arc. Cylindrical symmetry around the loading axis is assumed for the DAC sample.

almost randomly distributed whereas 100 and 110 align along the loading axis. This indicates that the planes that are preferentially oriented perpendicular to the loading axis change from (010) to (100) and (110) after annealing. It should be noted that our measurements are most sensitive to $77\text{--}90^\circ$ from the loading axis. However, the observed preferred orientation is significant considering the estimated uncertainty (Figure 4).

[16] Recently it has been suggested that the lattice preferred orientation of post-perovskite (i.e., $CaIrO_3$ type) may explain the seismic anisotropy at the lowermost mantle. While an earlier study proposed the (010) plane as the dominant slip plane [Iitaka *et al.*, 2004], more recent studies have proposed the (100) and (110) planes [Oganov *et al.*, 2005; Merkel *et al.*, 2006]. The pre-annealing texture observed for $CaIrO_3$ -type Mn_2O_3 is consistent with the former proposal. This texture may be induced by deformation under higher differential stresses. However, it is also possible that the texture is related to the phase transition: if displacement along the (010) plane occurs during the phase transition as inferred from the structural similarities between low- and high- P phases, the grains may be aligned along the (010) plane during the phase transition. Our post-annealing texture is consistent with more recent proposals [Oganov *et al.*, 2005; Merkel *et al.*, 2006]. This may represent the texture developed under lower differential stress conditions. However, we do not rule out a possibility that this texture results from the thermal annealing process [Green, 1967], although the temperature of the X-rayed area should not exceed a few hundred kelvins and our diffraction patterns indicate no significant recrystallization during annealing. We note that one of the recent proposals is based on measurements for $MgGeO_3$ post-perovskite after heating to 1600 K [Merkel *et al.*, 2006]. Our observation demonstrates that the texture of the $CaIrO_3$ type can be affected by phase transition and heating as well as differential stresses.

[17] **Acknowledgments.** We thank C. T. Prewitt, J. B. Evans, H. W. Green, S. Karato, T. S. Duffy, and an anonymous reviewer for helpful

comments to improve this paper. This work was performed at GSECARS which is supported by NSF, DOE, and the State of Illinois.

References

- Badro, J., G. Fiquet, V. V. Struzhkin, M. Somayazulu, H.-K. Mao, G. Shen, and T. L. Bihan (2002), Nature of the high-pressure transition in Fe_2O_3 hematite, *Phys. Rev. Lett.*, *89*, doi:10.1103/PhysRevLett.89.205504.
- Bunge, H.-J. (1983), *Texture Analysis in Materials Science: Mathematical Methods*, Elsevier, New York.
- Burns, R. G. (1993), *Mineralogical Applications of Crystal Field Theory*, Cambridge Univ. Press, New York.
- Funamori, N., and R. Jeanloz (1997), High-pressure transformation of Al_2O_3 , *Science*, *278*, 1109–1111.
- Geller, S. (1971), Structures of α - Mn_2O_3 , $(Mn_{0.98}Fe_{0.017})_2O_3$ and relation to magnetic ordering, *Acta Crystallogr., Sect. B Struct. Sci.*, *27*, 821–828.
- Green, H. W. (1967), Quartz: Extreme preferred orientation produced by annealing, *Science*, *157*, 1444–1447.
- Hammersley, A. P. (1997), Fit2d: An introduction and overview, internal report, Eur. Synchrotron Radiat. Facil., Grenoble, France.
- Holland, T. J. B., and S. A. T. Redfern (1997), Unit cell refinement from powder diffraction data: The use of regression diagnostics, *Mineral. Mag.*, *61*, 65–77.
- Iitaka, T., K. Hirose, K. Kawamura, and M. Murakami (2004), The elasticity of the $MgSiO_3$ post-perovskite phase in the Earth's lowermost mantle, *Nature*, *430*, 442–445.
- Larson, A. C., and R. B. Von Dreele (1988), GSAS manual, *Tech. Rep. LAUR 86-748*, Los Alamos Natl. Lab., Los Alamos, N. M.
- Lin, J.-F., O. Degtyareva, C. T. Prewitt, P. Dera, N. Sata, E. Gregoryanz, H.-K. Mao, and R. J. Hemley (2004), Crystal structure of a high-pressure/high-temperature phase of alumina by in situ x-ray diffraction, *Nat. Mater.*, *3*, 389–393.
- Mao, H.-K., J. Xu, and P. M. Bell (1986), Calibration of the ruby pressure gauge to 800 kbar under quasihydrostatic conditions, *J. Geophys. Res.*, *91*, 4673–4676.
- Merkel, S., A. Kubo, L. Miyagi, S. Speziale, T. S. Duffy, H.-K. Mao, and H. R. Wenk (2006), Plastic deformation of $MgGeO_3$ post-perovskite at lower mantle pressures, *Science*, *311*, 644–646.
- Murakami, M., K. Hirose, K. Kawamura, N. Sata, and Y. Ohishi (2004), Post-perovskite phase transition in $MgSiO_3$, *Science*, *304*, 855–858.
- Oganov, A. R., and S. Ono (2004), Theoretical and experimental evidence for a post-perovskite phase of $MgSiO_3$ in Earth's D' layer, *Nature*, *430*, 445–448.
- Oganov, A. R., and S. Ono (2005), The high-pressure phase of alumina and implications for Earth's D'' layer, *Proc. Natl. Acad. Sci. U. S. A.*, *102*, 10,828–10,831.
- Oganov, A. R., R. Martonak, A. Laio, P. Raiteri, and M. Parrinello (2005), Anisotropy of Earth's D'' layer and stacking faults in the $MgSiO_3$ post-perovskite phase, *Nature*, *438*, 1142–1144.
- Ono, S., and Y. Ohishi (2005), In situ x-ray observation of phase transformation in Fe_2O_3 at high pressures and high temperatures, *J. Phys. Chem. Solids*, *66*, 1714–1720.
- Ono, S., T. Kikegawa, and Y. Ohishi (2004), High-pressure phase transition of hematite, Fe_2O_3 , *J. Phys. Chem. Solids*, *65*, 1527–1530.
- Prewitt, C. T., R. D. Shannon, D. B. Rogers, and A. W. Sleight (1969), The C rare earth oxide-corundum transition and crystal chemistry of oxides having the corundum structure, *Inorg. Chem.*, *8*, 1985–1993.
- Reid, A. F., and A. E. Ringwood (1969), High-pressure scandium oxide and its place in the molar volume relationships of dense structures of M_2X_3 and ABX_3 type, *J. Geophys. Res.*, *74*, 3238–3252.
- Robinson, K., G. V. Gibbs, and P. H. Ribbe (1971), Quadratic elongation: A quantitative measure of distortion in coordination polyhedra, *Science*, *172*, 567–570.
- Shim, S.-H., T. S. Duffy, R. Jeanloz, and G. Shen (2004a), Stability and crystal structure of $MgSiO_3$ perovskite to the core-mantle boundary, *Geophys. Res. Lett.*, *31*, L10603, doi:10.1029/2004GL019639.
- Shim, S.-H., T. S. Duffy, R. Jeanloz, C.-S. Yoo, and V. Iota (2004b), Raman spectroscopy and x-ray diffraction of phase transitions in Cr_2O_3 to 61 GPa, *Phys. Rev. B*, *69*, doi:10.1103/PhysRevB.69.14.4107.
- Syono, A., T. Yagi, K. Kusaba, T. Ono, N. Shimoda, K. Fukuoka, and T. Suzuki (1985), Pressure-induced phase transitions in transition metal oxides Mn_2O_3 and $LiTiO_3$, paper presented at Japanese High-Pressure Conference, Jpn. Soc. of High Pressure Sci. and Technol., Tokushima, Japan.
- Thomson, K. T., R. M. Wentzcovitch, and M. S. T. Bukowski (1996), Polymorphs of alumina predicted by first principles: putting pressure on the ruby pressure scale, *Science*, *274*, 1880–1882.

Yamanaka, T., T. Nagai, T. Okada, and T. Fukuda (2005), Structure changes of Mn_2O_3 under high pressure and pressure-induced transition, *Z. Kristallogr.*, 220, 938–945.

V. B. Prakapenka, Bldg. 434A, Argonne National Laboratory, Argonne, IL 60439, USA.

J. Santillán, Ahura Corporation, 46 Jonspin Road, Wilmington, MA 01887, USA.

G. Shen, HPCAT, Bldg. 434E, Argonne National Laboratory, Argonne, IL 60439, USA.

S.-H. Shim, Department of Earth, Atmospheric, and Planetary Sciences, Massachusetts Institute of Technology, Cambridge, MA 02139, USA. (sangshim@mit.edu)